Validation of a Multimodality Flow Phantom and Its Application for Assessment of Dynamic SPECT and PET Technologies

Hanif Gabrani-Juma, Owen J. Clarkin, Amir Pourmoghaddas, Brandon Driscoll, R. Glenn Wells, *Member, IEEE*, Robert A. deKemp, *Member, IEEE*, and Ran Klein*, *Member, IEEE*

***Abstract*— Simple and robust techniques are lacking to assess performance of flow quantification using dynamic imaging. We therefore developed a method to qualify flow quantification technologies using a physical compartment exchange phantom and image analysis tool. We validate and demonstrate utility of this method using dynamic PET and SPECT. Dynamic image sequences were acquired on two PET/CT and a cardiac dedicated SPECT (with and without attenuation and scatter corrections) systems. A two-compartment exchange model was fit to image derived time-activity curves to quantify flow rates. Flowmeter measured flow rates (20-300 mL/min) were set prior to imaging and were used as reference truth to which image derived flow rates were compared. Both PET cameras had excellent agreement with truth ($r^2 > 0.94$). High-end PET had no significant bias ($p > 0.05$) while lower-end PET had minimal slope bias (wash-in and wash-out slopes were 1.02 and 1.01) but no significant reduction in precision relative to high-end PET (<15% vs. <14% limits of agreement, $p > 0.3$). SPECT (without scatter and attenuation corrections) slope biases were noted (0.85 and 1.32) and attributed to camera saturation in early time frames. Analysis of washout rates from non-saturated, late time frames resulted in excellent agreement with truth ($r^2 = 0.98$, slope = 0.97). Attenuation and scatter corrections did not significantly impact SPECT performance. The proposed phantom, software and quality assurance paradigm can be used to qualify imaging instrumentation and protocols for quantification of kinetic rate parameters using dynamic imaging.**

***Index Terms*— Flow, PET, Phantom, SPECT.**

Manuscript received May 20, 2016; revised July 25, 2016 and August 2, 2016; accepted August 3, 2016. Date of publication August 11, 2016; date of current version December 29, 2016. This work was supported by grants from the Natural Science and Engineering Research Council for Canada (EGP 463188-14 & RGPGP 436149-2013). *Asterisk indicates corresponding author.*

H. Gabrani-Juma is with The Ottawa Hospital, Division of Nuclear Medicine, Ottawa, ON K1Y 4E9, Canada (e-mail: hjuma@toh.on.ca).

O. J. Clarkin is with the University of Ottawa Heart Institute, Cardiac Imaging Research Core Laboratory, Ottawa, ON K1Y 4W7, Canada.

A. Pourmoghaddas is with the University of Ottawa Heart Institute, National Cardiac PET Centre, Ottawa, ON K1Y 4W7, Canada.

B. Driscoll is with the Princess Margret Hospital, Department of Radiation Physics, Toronto, ON M5G 2M9, Canada.

R. G. Wells is with the University of Ottawa Heart Institute, Department of Medicine Ottawa, ON K1Y 4W7, Canada.

R. A. deKemp is with the University of Ottawa Heart Institute, National Cardiac PET Centre, Department of Medicine (Cardiology), Ottawa, ON K1Y 4W7, Canada.

*R. Klein is with The Ottawa Hospital, Division of Nuclear Medicine, Ottawa, ON K1Y 4E9, Canada (e-mail: rklein@toh.ca).

Digital Object Identifier 10.1109/TMI.2016.2599779

I. Introduction

QUANTIFICATION of physiologic function using non-invasive, medical imaging techniques can provide valuable insight for medical management of patients and for research applications. Dynamic imaging from time of introduction of a compound of interest (radio-tracer or contrast agent) and during its distribution in the body can be used to quantify the kinetic rates of physiologic function. New and existing imaging instrumentation and function quantification techniques require validation. Therefore, we sought to develop a method by which image derived kinetic rate measurements can be easily validated against a known reference (flow). In this work we present a flow phantom, software and quality assurance paradigm to evaluate imaging instrumentation and protocols for quantification of kinetic rate parameters. We demonstrate the application on nuclear imaging data; yet the methodology can be applied to other imaging modalities.

Nuclear imaging studies can offer unique non-invasive insight to physiologic function, and therefore have been applied to a wide range of organs and diseases. Over the past several decades, the kinetics of these functions can not only be imaged, but also quantified with high precision and accuracy [1]. More recently, functional quantification in 3D tomographs has been possible using single photon emission computed tomography (SPECT) and positron emission tomography (PET), but it has yet to be widely applied clinically [2], [3]. Nevertheless, PET is currently considered to be the gold-standard modality for non-invasive quantitative functional imaging and recent developments in SPECT technology (e.g. solid state, cardiac dedicated SPECT [4]–[8]) have fueled interest in its utility for this purpose. Other modalities such as x-ray computed tomography (CT) and magnetic resonance (MR) similarly utilize dynamic contrast enhancement (DCE) to quantify tissue perfusion and permeability [9].

The shift from relative imaging to absolute function quantification has enabled more sensitive and specific tools for analysis of planar imaging studies for clinical and research applications (e.g. renal function, gastric emptying). Novel tomographic applications include quantification of myocardial blood flow (MBF), treatment response monitoring in oncology and cellular metabolic activity [10], [11].

Physiologic function quantification is performed using dynamic imaging from the time of tracer administration and including bio-distribution and metabolism within the organ of interest. Tracer concentration time-activity curves (TACs) are measured from the dynamic image sequence usually using regions of interest in the image. Tracer-specific kinetic models (pharmaco-kinetic transport models) are used to describe the exchange of activity between the input organ (e.g. arterial blood) and the tissue or organ (e.g. myocardium). The kinetic modeling equation is fitted to the TACs to derive tracer exchange rate parameters between the model compartments.

Accurate TAC measurement requires precise imaging instrumentation that is able to correct for photon attenuation and scatter, and to quantify activity concentrations of the tracer (e.g. Bq/cc) over a wide range of magnitudes. In early time frames the tracer is concentrated in the input organ region (blood), but as the tracer distributes through the patient's body it is greatly diluted. Furthermore, with a short-lived radionuclide (e.g. Rubidium-82, half-life= 76 s) the activity may significantly decay over the course of the imaging session (several minutes to an hour).

As the medical imaging community moves towards dynamic imaging and routine functional quantification, a need has arisen to validate existing and new instrumentation for this application. Furthermore, standardization between instrumentation and imaging sites has not yet been established for multi-site imaging studies. Therefore, a need exists for a suitable physical phantom and image analysis software that could be used easily to validate a nuclear imaging camera for dynamic imaging for the purpose of quantitative compartmental model analysis.

Previously described phantoms attempted to reproduce the exchange and kinetics of organs with simulated organ physiology [12]–[14]. Tissue based and simple microvasculature phantoms have been explored to simulate organ kinetics [4], [7], [16]. While some previous phantoms have been successful when simulating perfusion at the microvasculature level, and representing the kinetics of a specific organ, the phantoms have not provided a simple, robust, and practical method for dynamic imaging and blood flow quantification validation over a wide range of flow rates and activity concentrations [12]. Thus we developed a relatively simple physical phantom for evaluation of a two-compartment model (also referred to as a 1-tissue-compartment model) of fluid exchange.

This work describes the phantom and demonstrates its use to validate two types of PET systems using rubidium-82 chloride and a cardiac dedicated SPECT system using technetium-99m pertechnetate.

II. Methods

A. Phantom Design

Our phantom was based on a Dynamic Contrast-Enhanced (DCE) computed tomography (CT) and magnetic resonance (MR) Phantom (Shelley Medical Imaging Technologies, London, Ontario, Canada) designed as a reference platform for validation of kinetic modeling parameters [17]. For this investigation the DCE phantom was modified for nuclear imaging applications, specifically PET and SPECT modalities.

The phantom consists of a closed cylinder perfused by a perforated tube enabling fluid exchange [12]. The phantom exchange cylinder (Ø = 5.0 cm, length = 10.0 cm) without the perforated tube has a total volume of 196 mL [12]. The perforated (10 sets of 2 holes Ø= 1.2 mm) fluid distribution tube (outer Ø= 6.35 mm, length= 114.3 cm) passes through the cylinder curved wall surface (inlet), is coiled along the interior of the phantom cylinder, and then passes through a second port at the opposite longitudinal end of the cylinder curved wall (outlet). The cylinder has a third port located on the end cap (distal to the inlet port) of the cylinder for outlet of the cylinder fluid. Excluding the volume of the coiled tube, the cylinder volume was measured at 160 mL.

A water-filled, torso shaped shell (2001 NEMA IEC Body Phantom by Data Spectrum Corp, Hillsborough, NC) contains the phantom's exchange cylinder providing a medium for photon scatter and attenuation [12]. Three ports on the shell pass the inlet and two outlet lines to connect to the external hardware as illustrated in Fig. 1. The shell was modified to incorporate a pressure release vent of the shell in case of a leak from the perfused inner components. During operation, an overflow container for the pressure release port may be monitored to indicate any leaking of the inner components.

A peristaltic pump (MasterFlex, Vernon Hills, IL) (RK-07551-20, pump head OF-77250-62) replaced the original pulsatile flow pump (required a glycerol solution for lubrication purposes) so the system could use tap water. The peristaltic pump is capable of 1-1000 mL/min flow rates (Q_{pump}).

A small diameter radio-tracer injection port was located either between the pump and phantom input, or upstream from the pump to simulate intravenous injection.

Flows through the cylinder and the exchange tubing (Q_{cyl} and Q_{tube} respectively [mL/min]) are varied using flow control valves on each outlet. The relative flow rates (R_{cyl} or R_{tube} respectively [%]) can be calculated as a percentage of the pump flow rate (Q_{pump}) as in equation 1. The total of Q_{cyl} and Q_{tube} by definition is equal to Q_{pump} and therefore $R_{cyl} + R_{tube} = 100\%$. The controlled flow through each valve (Q_{cyl} and Q_{tube}) is measured using flowmeters [17], which served as reference truth to which image derived flows were compared. During configuration of the phantom both valves were adjusted to achieve a desired R_{cyl}. At all times care was taken to avoid closing both valves simultaneously, which could result in over-pressuring the system.

$$Q_{pump} = Q_{cyl} + Q_{tube} = Q_{pump} \times \frac{R_{cyl}}{100} + Q_{pump} \times \frac{R_{tube}}{100} \quad (1)$$

To accommodate the limited spatial resolution of nuclear imaging (PET and SPECT), an interchangeable inlet line to the exchange cylinder was constructed using a PVC cylinder (Ø = 1.905 cm, length = 5.5 cm). The large inlet chamber enables image-derived sampling of input TACs with reduced partial volume loss. The modified phantom remains compatible with x-ray and magnetic resonance modalities.

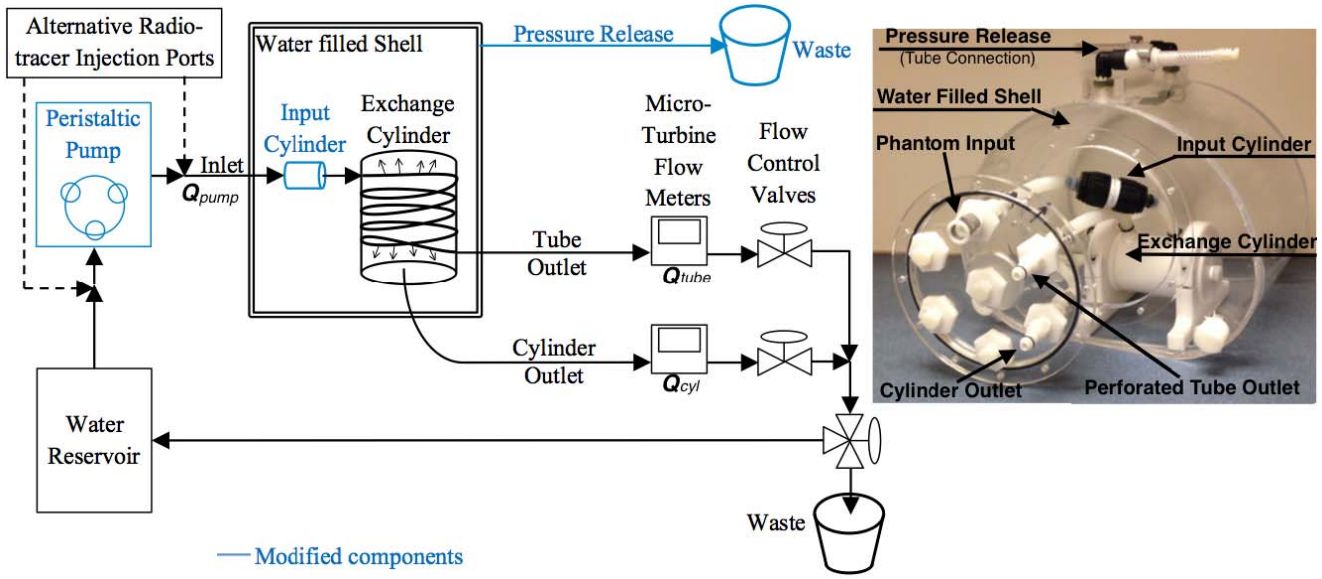

Fig. 1. System diagram (left) and photograph (right) of the phantom and external shell (double lines in diagram). Note that the radio-tracer injection port was relocated upstream or downstream from the pump (dashed lines).

TABLE I
IMAGE ACQUISITION PROTOCOL

Camera	Detector	Reconstruction Parameters	Corrections	Tracer	Injected Activity (MBq)
GE-690	LYSO	OSEM, 24 subsets, 4 iterations	Dead-time, Randoms, Attenuation, Scatter, Resolution, Decay	^{82}Rb	1800-2200
GE-600	BGO	OSEM 24 subsets, 4 iterations	Dead-time, Randoms, Attenuation, Scatter, Resolution, Decay	^{82}Rb	400-600
GE-530c NC	CZT	MLEM 100 iteration	Decay	^{99m}Tc	130-465
GE-530c AC	CZT	MLEM 100 iteration	Attenuation, Decay	^{99m}Tc	130-465
GE-530c ACSC	CZT	MLEM 100 iteration	Attenuation, Scatter, Decay	^{99m}Tc	130-465

B. Image Acquisition and Analysis

The nuclear imaging protocol was executed on two PET/CT cameras and a cardiac dedicated SPECT camera.

The phantom was imaged with ^{82}Rb on a GE Discovery 690 (GE690, GE Healthcare, Waukesha, WI), a PET/CT scanner with LYSO crystals, using a RubyFill^{TM} V2 infuser (Jubilant-DraxImage, Kirkland, Canada). Likewise, the phantom was imaged on a GE Discovery 600 (GE600, GE Healthcare, Waukesha, WI), a BGO crystal based PET/CT scanner. All ^{82}Rb injections were infused at a constant rate of activity over 30 second intervals [18]. Tracer activity was adjusted (Table I) to avoid scanner saturation [10], [19], [20]. The injection port was positioned upstream from the pump (between the pump and the water reservoir) to avoid over-pressure (>25 PSI induced by phantom pump) and automatic termination of the radio-tracer infusion by the ^{82}Rb infuser [18]. An 8-min list-mode scan was started manually when scanner true count rate exceeded 10 kcps (kilo-counts-per-second). The phantom position was not altered between scans, so a single CT attenuation correction (CTAC) image could be used for all ^{82}Rb scans.

Likewise, the phantom was imaged on a GE Discovery NM 530c (GE530 GE Healthcare, Haifa, Israel), a cardiac dedicated, cadmium-zinc-telluride (CZT) detector based SPECT camera without CT capabilities. The radio-tracer injection port was positioned immediately upstream from the phantom (and downstream from the pump) to reduce the chance of tracer adhering to the tubing [21], [22]. Hand injections of ^{99m}Tc- pertechnetate at an approximate constant rate over 30 seconds were used. List-mode data was acquired for 8 minutes and was manually started simultaneously with tracer administration. Prior to SPECT image acquisition, a CTAC image was acquired on a GE Infinia Hawkeye 4 SPECT-CT. The CTAC was imported to the console and manually registered to the SPECT data. SPECT images were reconstructed using three methods: without corrections (NC), with attenuation correction (AC) and with attenuation and scatter correction (ACSC). Scatter correction based on the dual-energy-window method was applied to the projection data using in house software prior to image reconstruction [23].

PET and SPECT list-mode data were binned into 15 frames (9 × 10 s, 3 × 30 s, 1 × 60 s, and 2 × 120 s) according to our standard clinical PET protocol. Reconstruction parameters and corrections are listed in Table I for each camera along with the tracer activities. All reconstructions were performed using the respective camera vendor provided software [23], [24].

On each camera the phantom was imaged twenty times with varying pump flow rates (Q_{pump} = 100, 200, 250 and 300 mL/min) and cylinder flow ratios (R_{cyl} = 20, 40, 60,

80 and 100%). At each run, the actual flowmeter readings (Q_{cyl} and Q_{tube}) were recorded and used as reference flow rates to which image derived values were compared. There was no background activity injected into the acrylic shell housing, and this was confirmed by sampling the background in post-reconstructed images.

GE690 data were used to validate the performance of the phantom. Subsequently performance of the lower-end GE600 PET and GE530 SPECT systems were evaluated in comparison to GE690 performance.

C. Image Analysis

Reconstructed dynamic images were processed using custom in-house developed software, derived from our clinical FlowQuant™ software (UOHI, Ottawa, Ontario Canada) for quantification of myocardial blood flow. The dynamic images were loaded into an interactive viewer where an operator selected the centers of the cylinder and inlet chamber (in late and early time frames respectively). To mitigate image spatial resolution related quantification losses, large regions of interest (ROIs) were automatically produced to include all pixels with >1% of the maximum intensity pixel within 8 cm (inlet) or 12 cm (cylinder) diameter spheres centered on the user selected points. Thus the resulting ROIs had a dilated form of the physical cylinders. Activity concentrations in each ROI were quantified by summing all the corresponding pixels values [Bq/cc], multiplying by the pixel volume, and then dividing them by the known chamber volumes [cc]. This approach was selected to reduce operator variability associated with defining cylindrical ROIs at oblique orientation angles. These ROIs sample activity in the dynamic image sequence to derive corresponding TACs, $C_{inletROI}(t)$ and $C_{cylROI}(t)$.

The TACs were processed using a kinetic model and a weighted (by frame length) least squares algorithm to derive measurements of the kinetics. A frequently used one-tissue-compartment (a.k.a. two-compartment) model was implemented to calculate the tracer exchange parameters of the dynamic data [25]. The tracer activity in the cylinder was modeled as:

$$C_{cyl}(t) = q_{in}e^{-q_{out}t} \otimes C_{tube}(t) \tag{2}$$

where $\otimes$ represents the discrete convolution operation, $C_{cyl}(t)$ represents the time-dependent tracer concentration in the cylinder, q_{in} represents the tracer wash-in rate to the cylinder [min^{-1}], and q_{out} represents the tracer wash-out rate from the cylinder [min^{-1}]. q_{in} and q_{out} are respectively analogous to K_1 and k_2 in kinetic-modeling of blood-tissue exchange. $C_{tube}(t)$ represents the tracer concentration in the perforated tube and can be estimated using the inlet chamber TAC $C_{inletROI}(t)$ using a transport *delay* [sec] which was incorporated into the compartment model as follows:

$$C_{tube}(t) = \begin{cases} C_{inletROI}(t - delay) & t > delay \\ 0 & t \le delay \end{cases} \tag{3}$$

Due to the presence of the perforated tube in the exchange cylinder (Fig. 3), large ROI and limited image spatial resolution, $C_{cylROI}(t)$ contained signals from both $C_{cyl}(t)$ and $C_{tube}(t)$. A signal mixing correction function [26] was implemented as shown in equation 4, where ISF represents the input signal fraction from the tubing and (1 – ISF) from the cylinder signal fraction. ISF is equivalent to the fractional blood volume [10] commonly used in the MBF literature to account for tissue arterial blood and signal spillover from the ventricle cavities. Thus, the complete kinetic model consisted of the following free parameters: q_{in}, q_{out}, ISF, and delay.

$$C_{CylROI} = (1 - ISF) \times C_{tube}(t) + ISF \times C_{cyl}(t) \tag{4}$$

D. Relationship Between Kinetic Model Parameters and Flow

The wash-in, q_{in} [min^{-1}], and wash-out, q_{out} [min^{-1}] rates were converted to absolute flow [mL/min] by multiplying the volume of the phantom cylinder (160 mL) as shown in equations 5 and 6. While no relationship between Q_{in} and Q_{out} was applied during kinetic modeling, the two parameters are expected to be equal as the liquid filled cylinder cannot expand or contract. Furthermore, these parameters are expected to be equal to Q_{Cyl}, the experimentally controlled flow through the cylinder. Thus the image derived Q_{in} and Q_{out} were evaluated against Q_{Cyl} as a reference.

$$Q_{in} = (Cylinder\ Volume) \times q_{in} \tag{5}$$

$$Q_{out} = (Cylinder\ Volume) \times q_{out} \tag{6}$$

E. Simulation Data

Cylinder concentration TAC were simulated using vendor provided software (Shelley Medical Technologies) [12] for the same Q_{in} and R_{cyl} values and corresponding image derived input TAC. The kinetic model was fitted using ISF and delay parameters set to zero as cylinder input-signal fraction (signal mixing) effects and transport delay were not simulated. Kinetic model derived Q_{in} and Q_{out} were compared to truth to validate kinetic model performance. The simulation software only simulated the exchange of fluid within the system, and did not simulate imaging, nor did it simulate noise. The activity used to simulate the TACs was not varied, as relative changes in radio-tracer concentrations were only dependent on rate of tracer exchange between the compartments (i.e. Q_{cyl}).

F. Quality Control

Dead-time correction factors from each PET scan were reviewed to ensure system count rates were below known saturation limits [19]. It was previously documented that the SPECT camera may momentarily turn off individual detectors when high count rates are present, as a hardware protection mechanism [22]. Since detector shut-off data were not readily available, list-mode derived, system total count rate curves (at 1-second intervals) were visually evaluated for periods of sudden reduced count statistics. These reductions were attributed to momentary detector shut-off at high count rates in the early, wash-in time frames. These list-mode data were rebinned (16 × 30 second intervals) using only the wash-out time frames (2.5 to 8 minutes), and were then sampled using the same cylinder ROI. A mono-exponential wash-out model was fitted to the TAC to derive Q_{out} (not Q_{in}).

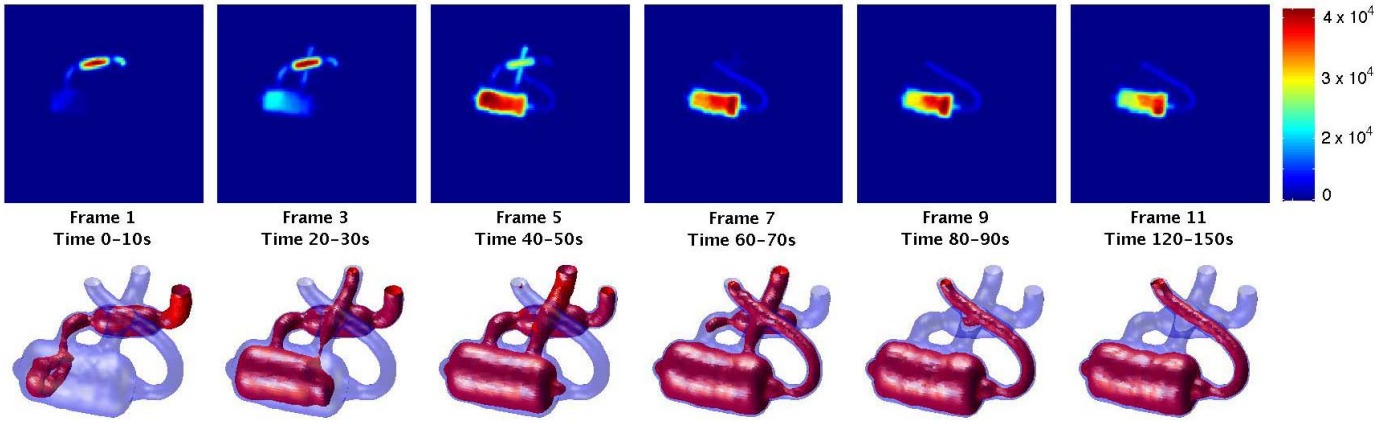

Fig. 2. Maximum intensity projection (top row) and 3D iso-surface rendering (bottom row) of dynamic images of the dynamic contrast phantom from a high count rate PET-CT scanner (GE690) showing the inlet chamber and fluid exchange cylinder.

TABLE II
IMAGE-DERIVED VERSUS PHYSICALLY MEASURED (FLOWMETERS) PHANTOM FLOW COMPARISONS

	r^2	Slope	Bias (relative to mean flows) (%)	Precision (95% LOA relative to mean flows) (%)
Q_{in} vs. Q_{cyl}				
Simulation	1.00	0.98	-1.4	1.5
GE690	0.97	1.02	0.3	11
GE600	0.95	1.02	9.8	14
GE530 NC	0.61	0.85	30	40
GE530 AC	0.80	0.82	15	28
GE530 ACSC	0.84	0.82	13	25
Q_{out} vs. Q_{cyl}				
Simulation	1.00	0.97	-1.9	1.9
GE690	0.94	0.99	2.3	14
GE600	0.94	1.01	10	15
GE530 NC	0.51	1.32	56	64
GE530 AC	0.94	1.37	29	30
GE530 ACSC	0.94	1.31	25	26

TABLE III
AGREEMENT AND VARIABILITY BETWEEN WASH-IN AND WASH-OUT (Q_{in} VS. Q_{out}) IMAGE-DERIVED PHANTOM FLOWS

	r^2	Slope	Bias (relative to mean flows) (%)	Precision (95% LOA relative to mean flows) (%)
Q_{in} vs. Q_{out}				
Simulation	1.00	0.99	-0.58	0.48
GE690	0.97	0.97	2.4	10
GE600	0.97	0.98	0.6	10
GE530 NC	0.91	1.61	27	38
GE530 AC	0.78	1.37	14	40
GE530 ACSC	0.82	1.36	13	37

G. Statistical Analysis

Agreement between measured Q_{cyl} and image derived Q_{in} and Q_{out} was evaluated using linear regression with accuracy determined by the corresponding slopes and intercepts. Bland-Altman analysis was used to evaluate systematic bias, and 95% confidence limits of agreement (LOA= 1.96 × standard deviation) were used as a metric of precision. Bias and LOA were both normalized to the average target flow rate for each series of scans (127.5 mL/min) and reported as a percentage. P-values <0.05 were considered statistically significant.

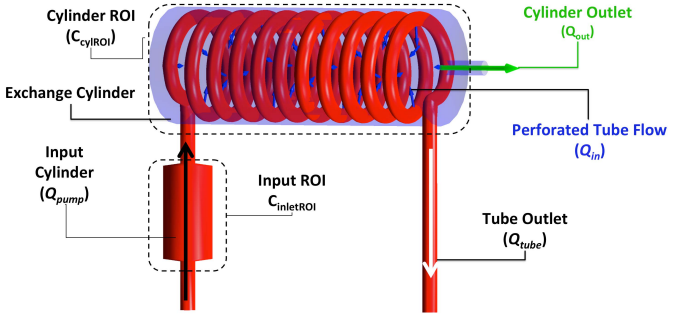

Fig. 3. Illustration of activity distribution route and ROI selection. Activity flows through the input cylinder (black arrow) into the exchange cylinder from the perforated tube coil (blue arrows) and exits the exchange cylinder via the cylinder outlet (green arrow) equal to the sum of inlet flows (blue arrows). Residual tube activity exits through the tube outlet (white arrow). The input and output ROIs were sampled to include the entire input cylinder (input TAC) and the exchange cylinder (output TAC).

III. RESULTS

A. Simulations

Excellent agreement was found between both Q_{in} and Q_{out} and the simulated Q_{cyl} with Pearson $r^2 = 1.00$ and near unity slopes (≥ 0.97). Q_{in} and Q_{out} parameters and measured flow rates had a small bias of -1.4% and -1.9% respectively (both $p < 0.01$). Precision was excellent with LOA<1.9%. Agreement between Q_{in} and Q_{out} was excellent (slope = 0.99 and $r^2 = 1.00$). A small bias was calculated with Q_{in} slightly higher than Q_{out} (+0.28%, $p < 0.01$). These results confirmed the accuracy of our kinetic analysis for subsequent imaging studies. The simulation results are summarized in Tables II and III.

B. Image Data

Sixty dynamic nuclear imaging scans were performed for this investigation - twenty times on each of the three cameras. A typical PET image of the modified phantom is presented in Fig. 2. Image derived and simulated TACs had similar shapes for PET, but less so for SPECT, as demonstrated in Fig. 4. During the course of imaging, no fluid passed

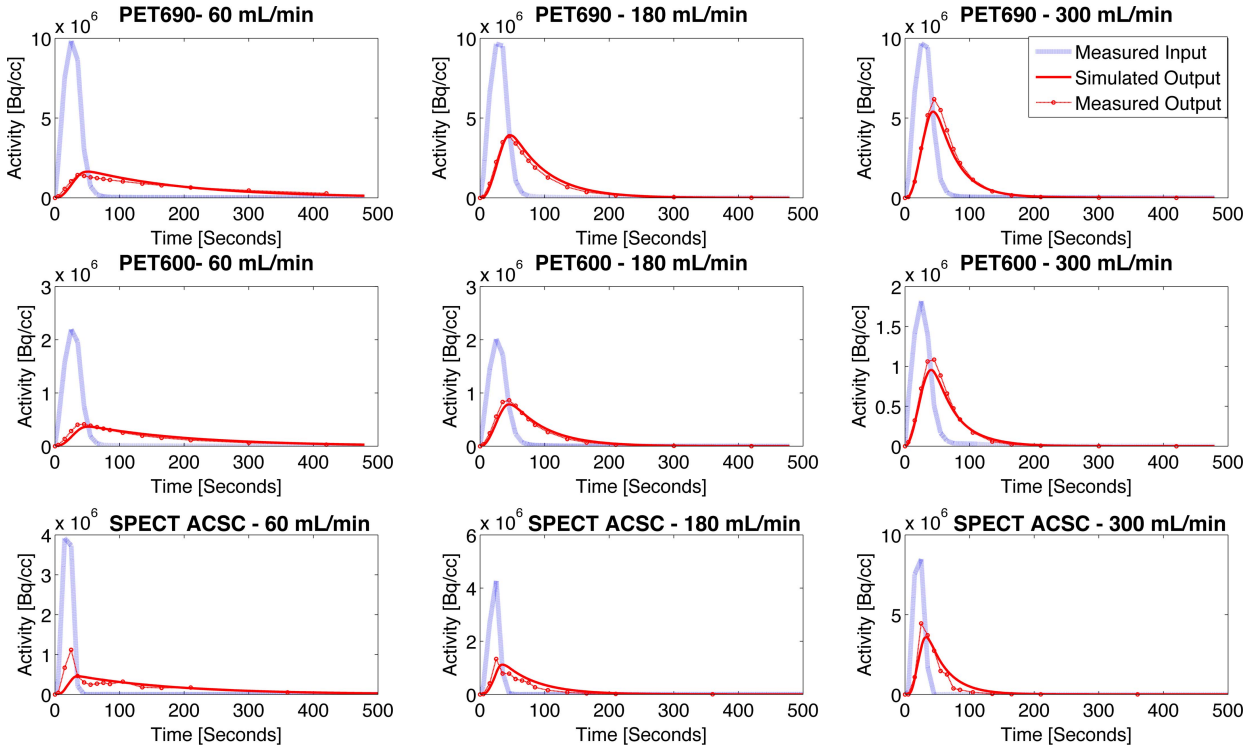

Fig. 4. Example image derived input (blue dotted) and output (red dashed line with markers) TACs from each scanner (GE690, GE600 and SPECT ACSC) compared with computer simulation output TACs (solid red) (Q_{in} = 300 mL/min and R_{cyl} = 20%, 60% and 100%). Note the wide range of activity concentrations even after radioactive decay correction. Also note good agreement of simulated and measured output TACs with PET, but less so with SPECT.

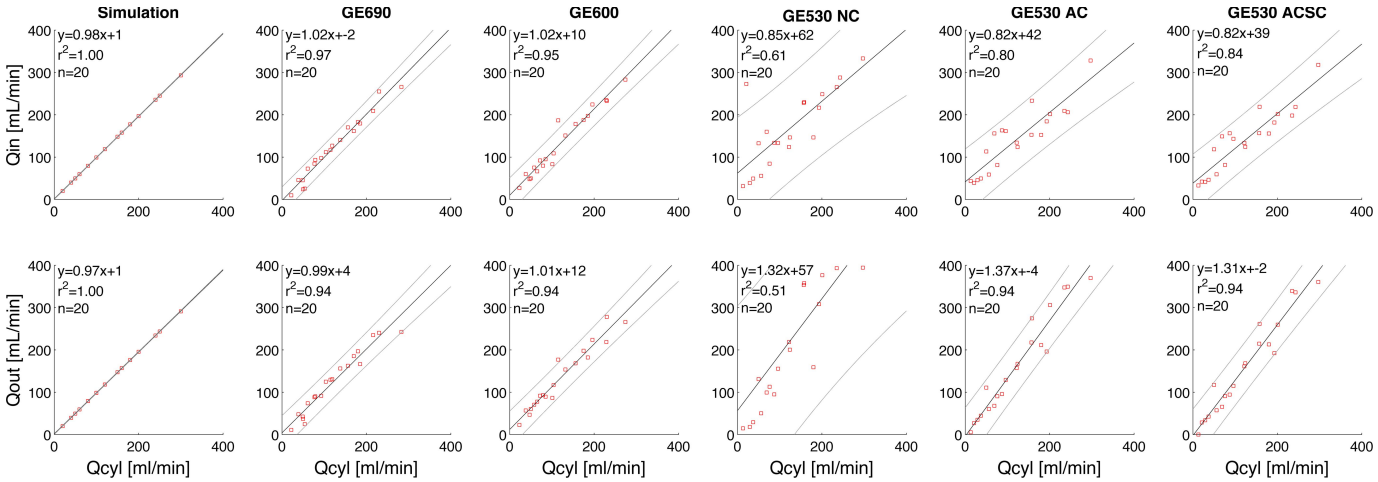

Fig. 5. Correlation of image derived (Q_{in} and Q_{out}) versus physically measured (flowmeter) phantom flow (Q_{cyl}) where solid grey lines represent the boundaries on the 95% confidence interval of the slope.

through the pressure release system. Count statistics in the FOV were greater than what is seen clinically. Scatter plots and correlation analysis of Q_{in} and Q_{out} versus Q_{cyl} are shown in Fig. 5 and summarized in Table II. Agreement between Q_{in} and Q_{out} is summarized in Table III.

C. PET

Visual inspection of the TACs confirmed no PET studies appeared saturated. GE690 image derived flow values had excellent accuracy and precision. Correlation with Q_{cyl} was strong ($r^2 > 0.94$) with no significant bias ($p > 0.45$) for either Q_{in} and Q_{out}, and respective LOA were 11% and 14%. No significant bias existed between Q_{in} and Q_{out} ($p = 0.32$) and there was excellent correlation ($r^2 = 0.97$) along with near unity slope (0.97). These results supported our understanding of the phantom, that ideally $Q_{in} = Q_{out} = Q_{cyl}$.

GE600 also had strong correlation ($r^2 > 0.94$) between both image-derived flows and the physically measured references. LOA for both flows was below 15% and not significantly different from GE690 results ($p > 0.30$). However, small

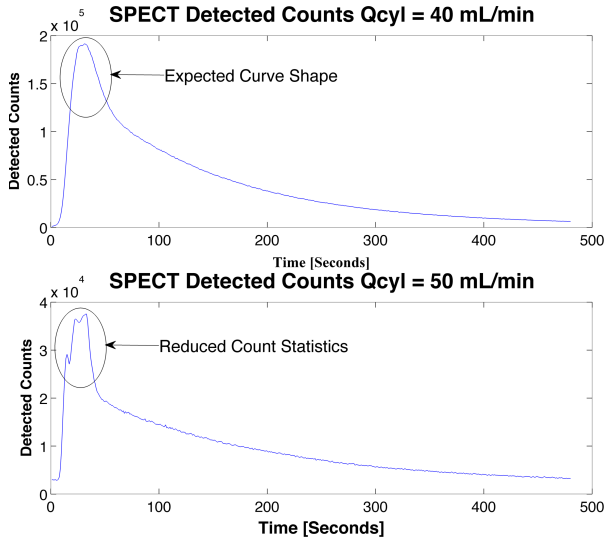

Fig. 6. Comparison of list-mode derived detector count rate curves of SPECT indicating unsaturated (left) and saturated (momentary loss of counts attributed to detector shut down) (right).

biases (<10%) were noted between image-derived and measured flows ($p < 0.05$), but no significant bias was found between the two image-derived flows ($p = 0.79$).

D. SPECT

GE530 data with no corrections had good correlations ($r^2 > 0.51$) but significant bias (30% and 56% for Q_{in} and Q_{out} respectively, $p < 0.01$). AC data biases improved to 15% and 29% ($p < 0.05$). The correlation value of Q_{in} versus Q_{cyl} ($r^2 = 0.80$) increased, but not significantly ($p = 0.22$); however, Q_{out} correlation ($r^2 = 0.94$) did improve significantly ($p < 0.001$). ACSC further reduced the bias between the image derived and measured flows to 13% and 25% ($p < 0.05$ versus NAC) and the precision tended to improve ($r^2 > 0.84$, $p < 0.1$). SC reduced the mean bias between the two image-derived flow rates to 13% ($p < 0.05$). Nevertheless, Q_{in} was consistently underestimated by 18% (slope = 0.82) and Q_{out} was overestimated by 31% (slope= 1.31) indicating an incremental improvement in precision, but not of accuracy.

Suspicion of saturation arose for some SPECT studies that had TACs with multiple peaks; this was supported by abrupt changes in list-mode derived count rates, as demonstrated in Fig. 6, and consistent with camera detector shutdown. Mono-exponential derived Q_{out} results from the late-phase images are shown in Fig. 7 demonstrating dramatic improvements in accuracy with $\leq$ 10% bias from unity slope and correlation values ($r^2 > 0.98$) not statistically different from those of PET ($p > 0.10$).

IV. Discussion

This work, to our knowledge, is the first of its kind to develop and validate the performance of a one-tissue-compartment (a.k.a two-compartment) model phantom for nuclear imaging that can be used to evaluate instrumentation on the merit of quantification of fluid exchange rate constants. The phantom is useful for evaluating instrumentation and image reconstruction techniques for the purpose of quantitative dynamic imaging and kinetic analysis of the images. We envision that this phantom may be useful for evaluating new imaging technologies for quantification and standardization of imaging practices across a diverse range of devices and imaging sites. Therefore, in accordance with the original design, all modifications to the phantom maintained compatibility with MR and CT applications.

A. PET

We first validated the phantom using a high-end PET system (GE690); where there was excellent accuracy between the image-derived and measured flow rates. The phantom behaved as expected, as a freely diffusible tracer exchange system, with near perfect agreement between wash-in, wash-out, and measured reference flow rates.

We then demonstrated the use of the phantom to evaluate performance of a lower-end PET (GE600) and a cardiac dedicated SPECT (GE530c). The lower-end PET system also had a high level of accuracy between image-derived and measured flow rates. A small but statistically significant bias (<10%) was observed on the GE600 studies, which was not present for the higher-end GE690 camera. There was no statistically significant difference in the correlation (r^2) of the two PET cameras ($p > 0.30$). Neither PET camera had statistically significant bias between the two image-derived flow rates (Q_{in} versus Q_{out}); consistent with the retention-free system design. We concluded that the two PET cameras have similar degrees of precision (LOA $p > 0.30$), but that the higher-end (GE690) may have slightly higher accuracy. The source of bias on the GE600 was not resolved, but may be associated with slightly inaccurate dead-time corrections in early time frame when operating at near peak count rates. Since the bias is apparent in both wash-in and wash-out rates, and there is no bias between these rates a correction factor could be applied, but was not the intention of this work.

B. SPECT

With developments in instrumentation and quantitative image reconstruction, the literature has demonstrated the ability to quantify physiologic function using SPECT [4]–[8], [27]. Our phantom results, using a single tissue-compartment kinetic model, suggest that the image acquisition protocol used for the SPECT system was suboptimal. Previous research has documented that the GE530c may momentarily shut down to protect electronics if detected activity exceeds a predetermined threshold [28]. Thus caution is required to avoid saturation of the camera electronics.

Using only the wash-out phase (excluding saturation affected data) of the SPECT image data and a mono-exponential wash-out model we were able to conclude that the GE530c is likely capable of similar degrees of accuracy and precision as the lower-end PET system for quantification of activity concentrations and kinetic parameters. In the case of our SPECT results, LOA is only an upper-bound measure of precision due to its dependence on slope bias and therefore

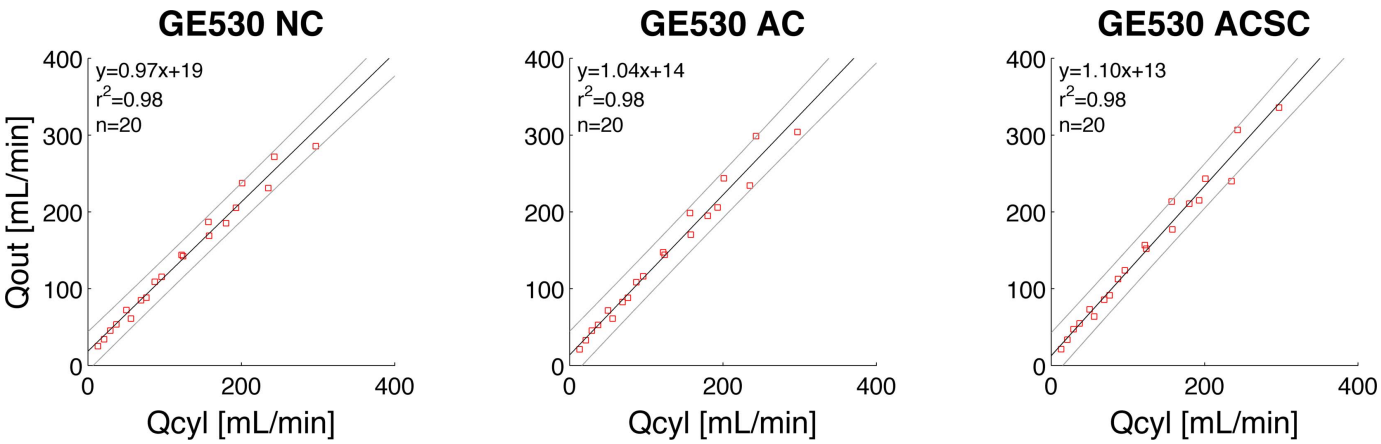

Fig. 7. Scatter plots of mono-exponential wash-out model derived out-flows (Q_{out}) from late phase (2.5-8 min post injection) SPECT images versus measured (flowmeter) reference (Q_{cyl}). The black and gray lines indicate the linear-regression and 95% confidence interval respectively.

we also reported r^2 as a measure of precision [29]. The mono-exponential wash-out precision with AC and ACSC did not significantly differ from that of NC. Previous investigation found that while AC and SC improved accuracy, image noise increases with these corrections [7]. Dynamic image reconstruction on the SPECT scanner is not vendor supported and required manual processing including our own implementation of scatter correction [23]. It is likely that future work could result in improved scatter correction. Furthermore, both corrections relied on manual alignment of emission and attenuation data with each data set individually, which is a potential source of error in the SPECT results, as opposed to accurate hardware alignment in the PET-CT hybrid system.

C. Limitations

One possible criticism of this phantom is that it is not physiologically complete. The phantom shell is smaller than typical cardiac patients resulting in less attenuation and scatter and better image quality. The phantom does not replicate the physiological function of capillary permeability, nor any contractile or respiratory motion. However, the phantom does accurately replicate the free exchange of fluid between compartments in a reproducible manner, as well as mixing of input (arterial) and output (tissue) signals in the organ ROI. Therefore, the phantom provides a simple and cost-effective gold standard by which quantitative imaging and analyses can be validated across various dynamic contrast and/or tracer imaging modalities.

D. Exchange Phantom Design

The phantom was designed with a perforated tube coil in order to achieve homogenous tracer distribution within the exchange cylinder. As demonstrated in Fig. 2, this was not completely achieved, as high activity concentration regions seemed to migrate from the start of the perforated tube (left of image) toward the cylinder outlet (right of image) over the course of imaging. Nevertheless, using a large ROI that encompassed the entire cylinder, non-uniform distribution could be accommodated. Future phantom designs may consider simpler designs with a single point of activity entry into the exchange chamber which may possibly be modeled using a simpler compartmental model that does not include input and output signal mixing.

E. Comparison to Clinical Data

Our group previously reported on short-term test-restest repeatability of MBF measurements using the same camera (GE690), infusion system and tracer kinetic model [30]. MBF values, which are related to K_1 after tracer extraction correction, are analogous to Q_{in} values in this work. In human studies, the 95% LOA was estimated at 20-25% while in this work we reported 11%. This can be explained by several confounding factors including physiologic variability in patients, non-linear extraction correction, partial volume effects, and the presence of cardiac and respiratory motion. Therefore, it is reasonable to conclude that the precision measurements obtained with the proposed phantom represent the best-case performance limit of the technology, and not the precision that can be reasonably achieved clinically.

While strict relationships between phantom flow measures and physiological flow parameters may be inaccurate, some analogies may be made. Flow to the exchange cylinder, Q_{pump}, corresponds to arterial blood flow to tissue. Flow into the cylinder, Q_{cyl}, is related to the tracer/contrast influx (wash in) across the capillary membrane into the extravascular space, which when normalized for the volume of the perfused tissue (cylinder volume = 196mL), can be compared to the permeability surface product (PS = $Q_{cyl}/196$ mL) [mL/min/mL] [9]. The flow percentage, R_{cyl} [%] is also an analogue to the contrast/tracer extraction-fraction expressed as a percentage (EF %). The phantom flow kinetics behaves in a similar fashion to a freely diffusible tracer such as ^{15}O-water, used routinely as the gold standard for flow quantification in PET imaging [31].

F. Use of the Phantom

This work confirms that Q_{Cyl} is the only parameter that influences wash-in and wash-out flow rates in the cylinder. Due to this property we achieved overlapping Q_{cyl} (e.g. 300 mL/min $R_{cyl} = 20\%$ and 100 mL/min $R_{cyl} = 60\%$).

Future validation experiments therefore may be simplified to include a single pump flow rate (e.g. 250 mL/min) and a range of flow ratios (e.g. $R_{cyl} = 10\%$ to 100% in increments of 15%), validating a wide range of flows with fewer measurements, while maintaining consistent transport delay from the injection port to the cylinder. Alternatively, consistent fluid exchange rates in the cylinder can be maintained while evaluating the variability of image derived flow values with pump flow rate and/or transport delay.

In this investigation, the tracer was injected as an extended 30-second bolus similar to our clinical ^{82}Rb protocol. Previous work on PET modalities has shown improvements for both accuracy and precision of image-derived flow measurements with the use of longer tracer injection times in a controlled animal model study [10]. This phantom provides a robust platform on which these effects can be further investigated. Likewise, future work may be warranted to determine the effects of tracer administration profiles in dynamic SPECT imaging [7], [25].

V. Conclusion

The dynamic imaging phantom was successfully adapted for use in dynamic PET and SPECT imaging while maintaining compatibility with CT and MR imaging. The performance of the phantom was validated using a high-performance PET scanner. Subsequently, the precision and accuracies of a second PET and a SPECT (wash-out only) for quantification of tracer exchange rates were evaluated. The phantom may be used to validate instrumentation and image reconstruction for quantification of physiological processes.

Acknowledgements

The phantom was provided by in-kind support from GE Healthcare. R. Glenn Wells collaborates with GE Healthcare on research projects and has received honoraria for speaking at GE Healthcare User Meetings. Robert deKemp and Ran Klein receive revenues from the sale of FlowQuant software and receive consulting fees and royalties from Jubilant-DraxImage for the sale of Rb PET technologies. No other potential conflicts relevant to this article were reported.

References

[1] S. Kaihara, T. K. Natarajan, C. D. Maynard, and H. N. Wagner, Jr., "Construction of a functional image from spatially localized rate constants obtained from serial camera and rectilinear scanner data," *Radiology*, vol. 93, no. 6, pp. 1345–1348, Dec. 1969.

[2] M. C. Ziadi, R. A. deKemp, and R. S. B. Beanlands, "Quantification of myocardial perfusion: What will it take to make it to prime time?" *Curr. Cardiovas. Imag. Rep.*, vol. 2, no. 3, pp. 238–249, Jun. 2009.

[3] E. V. Garcia, "Are absolute myocardial blood flow PET measurements ready for clinical use?" *J. Nucl. Cardiol.*, vol. 21, no. 5, pp. 857–858, Oct. 2014.

[4] S. Ben-Haim *et al.*, "Quantification of myocardial perfusion reserve using dynamic SPECT imaging in humans: A feasibility study," *J. Nucl. Med.*, vol. 54, no. 6, pp. 873–879, Jun. 2013.

[5] R. Klein *et al.*, "Feasibility and operator variability of myocardial blood flow and reserve measurements with ^{99m}Tc-sestamibi quantitative dynamic SPECT/CT imaging," *J. Nucl. Cardiol.*, vol. 21, no. 6, pp. 1075–1088, Dec. 2014.

[6] B. Hsu *et al.*, "Quantitation of myocardial blood flow and myocardial flow reserve with ^{99m}Tc-sestamibi dynamic SPECT/CT to enhance detection of coronary artery disease," *Eur. J. Nucl. Med. Mol. Imag.*, vol. 41, no. 12, pp. 2294–2306, Dec. 2014.

[7] R. G. Wells *et al.*, "Dynamic SPECT measurement of absolute myocardial blood flow in a porcine model," *J. Nucl. Med.*, vol. 55, no. 10, pp. 1685–1691, Oct. 2014.

[8] H. Cochet *et al.*, "Absolute quantification of left ventricular global and regional function at nuclear MPI using ultrafast CZT SPECT: Initial validation versus cardiac MR," *J. Nucl. Med.*, vol. 54, no. 4, pp. 556–563, Apr. 2013.

[9] C. A. Cuenod and D. Balvay, "Perfusion and vascular permeability: Basic concepts and measurement in DCE-CT and DCE-MRI," *Diagnostic Intervent. Imag.*, vol. 94, no. 12, pp. 1187–1204, Dec. 2013.

[10] R. Klein, R. S. B. Beanlands, and R. A. deKemp, "Quantification of myocardial blood flow and flow reserve: Technical aspects," *J. Nucl. Cardiol.*, vol. 17, no. 4, pp. 555–570, Aug. 2010.

[11] R. Boellaard, "Standards for PET image acquisition and quantitative data analysis," *J. Nucl. Med.*, vol. 50, no. 1, pp. 11S–20S, May 2009.

[12] B. Driscoll, H. Keller, and C. Coolens, "Development of a dynamic flow imaging phantom for dynamic contrast-enhanced CT," *Med. Phys.*, vol. 38, no. 8, pp. 4866–4880, Aug. 2011.

[13] T. N. Teslow and R. A. Robb, "X-ray computed tomographic (CT) phantom designed for the development of techniques for measurement of myocardial perfusion," *Phys. Med. Biol.*, vol. 36, no. 10, p. 1407, Oct. 1991.

[14] A. J. Hindle and A. C. Perkins, "A perfusion phantom for the evaluation of ultrasound contrast agents," *Ultrasound Med. Biol.*, vol. 20, no. 3, pp. 309–314, 1994.

[15] B. Ebrahimi, S. D. Swanson, and T. E. Chupp, "A microfabricated phantom for quantitative MR perfusion measurements: Validation of singular value decomposition deconvolution method," *IEEE Trans. Biomed. Eng.*, vol. 57, no. 11, pp. 2730–2736, Nov. 2010.

[16] U. Haberland, J. Cordes, M. Lell, N. Abolmaali, and E. Klotz, "A biological phantom for contrast-media-based perfusion studies with CT," *Invest. Radiol.*, vol. 44, no. 10, pp. 676–682, Oct. 2009.

[17] B. Driscoll, H. Keller, D. Jaffray, and C. Coolens, "Development of a dynamic quality assurance testing protocol for multisite clinical trial DCE-CT accreditation," *Med. Phys.*, vol. 40, no. 8, p. 81906, Aug. 2013.

[18] R. Klein, A. Adler, R. S. Beanlands, and R. A. deKemp, "Precision-controlled elution of a 82Sr/82Rb generator for cardiac perfusion imaging with positron emission tomography," *Phys. Med. Biol.*, vol. 52, no. 3, pp. 659–673, Feb. 2007.

[19] J. M. Renaud *et al.*, "Characterization of 3D PET systems for accurate quantification of myocardial blood flow," *J. Nucl. Med.*, Aug. 18, 2016.

[20] D. Tout, C. M. Tonge, S. Muthu, and P. Arumugam, "Assessment of a protocol for routine simultaneous myocardial blood flow measurement and standard myocardial perfusion imaging with rubidium-82 on a high count rate positron emission tomography system," *Nucl. Med. Commun.*, vol. 33, no. 11, pp. 1202–1211, Nov. 2012.

[21] J. Roy, M. McMahon, and D. Gilmore, "Residual syringe activity: Is there a need for concern?" *J. Nucl. Med.*, vol. 51, no. 2, p. 2111, May 2010.

[22] T. N. Swanson, D. T. Troung, A. Paulsen, C. B. Hruska, and M. K. O'Connor, "Adsorption of ^{99m}Tc-sestamibi onto plastic syringes: Evaluation of factors affecting the degree of adsorption and their impact on clinical studies," *J. Nucl. Med. Technol.*, vol. 41, no. 4, pp. 247–252, Dec. 2013.

[23] A. Pourmoghaddas, K. Vanderwerf, T. D. Ruddy, and R. G. Wells, "Scatter correction improves concordance in SPECT MPI with a dedicated cardiac SPECT solid-state camera," *J. Nucl. Cardiol.*, vol. 22, no. 2, pp. 334–343, Apr. 2014.

[24] V. Bettinardi *et al.*, "Physical performance of the new hybrid PET/CT discovery-690," *Med. Phys.*, vol. 38, no. 10, pp. 5394–5411, Oct. 2011.

[25] R. Klein *et al.*, "Intra- and inter-operator repeatability of myocardial blood flow and myocardial flow reserve measurements using rubidium-82 pet and a highly automated analysis program," *J. Nucl. Cardiol.*, vol. 17, no. 4, pp. 600–616, Aug. 2010.

[26] G. D. Hutchins, J. M. Caraher, and R. Raylman, "A region of interest strategy for minimizing resolution distortions in quantitative myocardial PET studies," *J. Nucl. Med.*, vol. 33, no. 6, pp. 1243–1250, Jun. 1992.

[27] W. L. Duvall *et al.*, "Reduced isotope dose with rapid SPECT MPI imaging: Initial experience with a CZT SPECT camera," *J. Nucl. Cardiol.*, vol. 17, no. 6, pp. 1009–1014, Dec. 2010.

[28] M. Bocher *et al.*, "A fast cardiac gamma camera with dynamic SPECT capabilities: Design, system validation and future potential," *Eur. J. Nucl. Med. Molecular Imag.*, vol. 37, no. 10, pp. 1887–1902, Oct. 2010.

[29] J. W. Bartlett and C. Frost, "Reliability, repeatability and reproducibility: Analysis of measurement errors in continuous variables," *Ultrasound Obstetrics Gynecol.*, vol. 31, no. 4, pp. 466–475, Apr. 2008.

[30] M. Efseaff, R. Klein, M. C. Ziadi, R. S. Beanlands, and R. A. deKemp, "Short-term repeatability of resting myocardial blood flow measurements using rubidium-82 PET imaging," *J. Nucl. Cardiol.*, vol. 19, no. 5, pp. 997–1006, Oct. 2012.

[31] PET: Is myocardial flow quantification a clinical Reality?—Springer, accessed on Nov. 18, 2015. [Online]. Available: http://link.springer.com.proxy.library.carleton.ca/article/10.1007/s12350-012-9588-8